Constitutive Models for Rubber XII – Marano et al (eds)

A visco-hyperelastic numerical model for the dynamic behaviour of rubbers

L. Andena, F. Cotta Ramusino, S. Tagliabue & S. Zalaffi
Dipartimento di Chimica, materiali e ingegneria chimica, Politecnico di Milano, Milan, Italy
E[4]SPORT (Engineering for Sport) lab, Politecnico di Milano, Milan, Italy

ABSTRACT: In this work, a visco-hyperelastic numerical model is proposed, based on the decoupling of the strain and time dependent contributions. Four different rubber blends, used for the production of athletics tracks, have been experimentally characterized in compression under varying loading histories. A robust identification procedure provided reliable constitutive parameters to be implemented in the numerical simulations. Model predictions have been validated against the outcome of impact tests performed on the different materials using an Artificial Athlete. Results demonstrate that the presence of a viscoelastic component grants a more accurate description of the energy return characteristics of rubbers under dynamic conditions.

1 INTRODUCTION

Rubbers have been used for a long time in many different fields, with applications exploiting their unique set of properties. Design with elastomeric materials (which typically incorporate a large amount of fillers) is challenging because of their intrinsically non-linear viscoelastic mechanical behaviour. While the scientific and technical literature offer a relatively large abundance of models suitable for rubbers (e.g. Bazkiaei et al. 2020, Busfield et al. 2000, Carleo et al. 2018, De Tommasi et al. 2019) their adoption has been so far limited in many industrial sectors, including sports surfaces (Carré et al. 2006, Cole et al. 2018, Kobayashi & Yukawa 2011, Thomson et al. 2001) which will be the focus of the present work.

Synthetic sport surfaces have nowadays replaced mineral or grass ones in top level competitions, thanks to the advantages they provide in terms of performance, maintenance needs and durability. To fully exploit these benefits, modern athletics tracks typically consist of at least two layers: the top finishing, which is embossed and responsible for grip, durability and appearance of the surface; and the bottom base one, often structured with some kind of honeycomb pattern, whose function is to provide optimal shock absorption and energy return characteristics. Each layer is typically composed by a different blend of rubbers, including natural (NR), styrene-butadiene (SBR), ethylene propylene diene monomer (EPDM) rubbers, with a large amount of fillers.

The optimization of the geometry and composition of athletics tracks in view of their safety and performance can be driven by numerical models, firmly rooted in the mechanical characterization of the dynamic properties of their constituent materials. This approach has been followed in a series of previous works (Andena et al. 2014, 2015, 2016, 2018a, b, Benanti et al. 2013), leading to the development of a 3D finite element (FE) hyperelastic model, whose parameters were identified from lab tests performed on the track constituents. The model proved itself able to accurately predict the shock absorption characteristics of a given track, measured experimentally by performing test using an Artificial Athlete (AA) apparatus as specified by the relevant EN 14808 standard.

Yet, the lack of a dissipative component in the model limits its ability to correctly evaluate the energy return characteristics of the surface, which are essential in determining the athletes' performance (Baroud et al. 1999, McMahon et al. 1979, Nigg & Yeadon 1987). To overcome this limitation, the existing constitutive model has been enriched in the present work with a dissipative, viscoelastic component.

2 THEORETICAL BACKGROUND

The chosen approach (Goh et al. 2004) assumes that material strain and time dependence can be decoupled, so that the stress σ at a given stretch λ and time t can be expressed by:

$$\sigma(\lambda, t) = \sigma_0(\lambda) g(t) \tag{1}$$

DOI: 10.1201/9781003310266-45

$\sigma_0(\lambda)$ represents the instantaneous stress-stretch relationship that can be derived by differentiation of an appropriate hyperelastic potential of choice, such as Ogden or Van der Waals, given by Equations 2 and 3 under the hypothesis of incompressible material:

$$U = \sum_{i=1}^{N} \frac{2 \cdot \mu_i}{\alpha_i^2}\left(\lambda_1^{\alpha_i} + \lambda_2^{\alpha_i} + (\lambda_1\lambda_2)^{-\alpha_i} - 3\right) \quad (2)$$

$$U = -\psi\left\{ \begin{array}{c} (\lambda_m^2 - 3)\left[\ln\left(1 - \sqrt{\frac{I_1-3}{\lambda_m^2-3}}\right) + \sqrt{\frac{I_1-3}{\lambda_m-3}}\right] \\ + \frac{2}{3}a\left(\frac{I_1-3}{2}\right)^{\frac{3}{2}} \end{array} \right\} \quad (3)$$

α_i, μ_i ψ, λ_m and a are material constants, while I_1 is the first invariant of the deviatoric strain tensor (the dependence of U on the second invariant was neglected).

$g(t)$ in turn is a time-dependent function based on a Prony series, as given by Equations 4 and 5:

$$g(t) = g_\infty + \sum_{i=1}^{N} g_i \exp\left(-\frac{t}{\tau_i}\right) \quad (4)$$

$$g_\infty + \sum_{i=1}^{N} g_i = 1 \quad (5)$$

$g_\infty\sigma_0(\lambda)$ being the long-term equilibrium stress for a given applied stretch, λ.

The advantage of the present approach is that the convolution integral of the viscoelastic problem can be separated into its long-term elastic and viscoelastic contributions:

$$\sigma(t) = \int_o^t g(t-s)\frac{d\sigma_0(\lambda)}{ds}ds \quad (6)$$

$$\sigma(t) = \int_0^t \left(g_\infty + \sum_{i=1}^{N} g_i\, e^{-\frac{t-s}{\tau_i}}\right)\frac{d\sigma_0(\lambda)}{ds}ds \quad (7)$$

$$\sigma(t) = g_\infty\sigma_0(t) + \sum_{i=1}^{N}\int_0^t g_i e^{-\frac{t-s}{\tau_i}}\frac{d\sigma_0(s)}{ds}ds \quad (8)$$

$$\sigma(t) = g_\infty\sigma_0(t) + \sum_{i=1}^{N} h_i(t) \quad (9)$$

While Equations 5-7 cannot be solved analytically (except for specific hyperelastic potentials and loading histories), Equation 8 can be solved numerically for any form of $\sigma_0(\lambda)$ by using the well-known Taylor algorithm, whose finite time increment scheme is widely used in finite element analyses.

3 EXPERIMENTAL

The materials investigated were 4 rubber mixtures (NR/SBR/EPDM/filler), typically used for the top finishing (F1, F2) and bottom base (B1, B2) layers of running tracks. Circular samples of 18 mm radius were cut from 4.7 mm thick plates which had been compression molded at 165°C for 10 minutes; the density of the materials produced ranged between 1250 and 1400 kg/m^3.

Uniaxial compression tests were performed down to a stretch of 0.6, using polytetrafluoroethylene (PTFE) film as a lubricant between the metal plates and the rubber samples. Tests were run at varying constant displacement speed, corresponding to nominal stretch rates of 0.006, 0.06 and 0.6 s^{-1}. Additionally, relaxation tests were performed following a ramp at 0.06 s^{-1} down to stretches of 0.9 and 0.7, and then keeping the stretch fixed for 300 s.

For validation purposes, 30 mm side square samples cut from a complete track were also characterized in compression, also at nominal stretch rates of 0.006, 0.06 and 0.6 s^{-1}, down to an apparent stretch of 0.6. The samples were composed of calendered top and bottom layers, bonded together by co-vulcanization: the top one had a thickness of 4.6 mm and was composed of material F2; the bottom one, having a thickness of 8 mm, was made of material B1 and bore a hexagonal honeycomb pattern, as visible in Figure 1. The production process resulted in materials having a significant residual porosity, so that the apparent densities of the top and bottom layer were about 1000 and 750 kg/m^3, respectively. The testing direction was perpendicular to the layer plane.

Each test was repeated on 3 different samples for each material/condition.

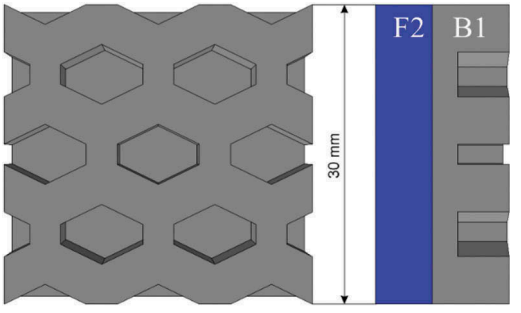

Figure 1. Complete track sample, as represented in the 3D FE model in Abaqus.

4 CONSTITUTIVE MODEL CALIBRATION

Typical experimental data is shown in Figure for material B1. The numerical solution of Equation 8 was fitted to the complete dataset available for each material via a least squares method, implemented

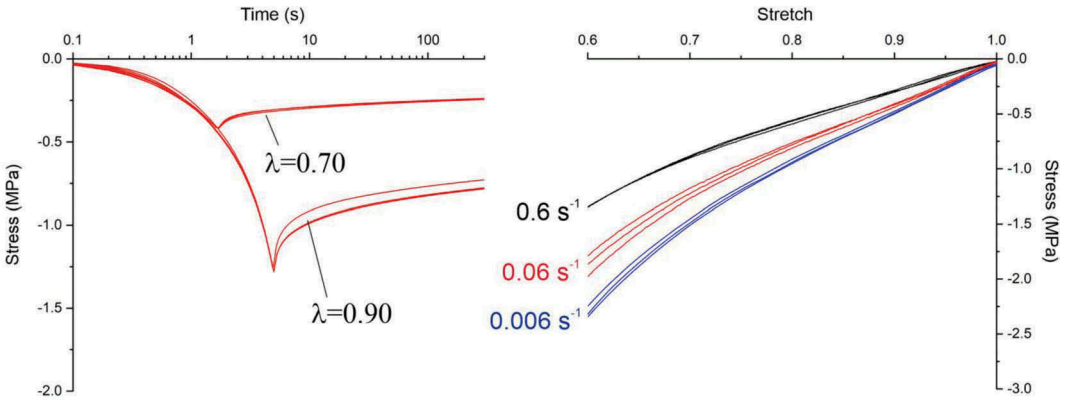

Figure 2. Experimental data for material B1: stress relaxation (left); variable constant strain rate (right).

Table 1. Identified model parameters. For each material, 4-terms and 6-terms Prony series are considered.

Ogden	μ_1	α_1	μ_2	α_2	g_1	g_2	g_3	g_4	g_5	g_6
	MPa		MPa		τ_1=0.003s	τ_2=0.03s	τ_3=0.3s	τ_4=3s	τ_5=30s	τ_6=300s
F1	14.59	2.75	-11.58	0.74	-	-	0.03	0.21	0.16	0.07
	23.19	2.51	-19.25	0.97	0.28	0.00	0.13	0.14	0.11	0.05
F2	3.33	2.62	-	-	-	-	0.20	0.19	0.10	0.06
	4.05	2.57	-	-	0.06	0.17	0.11	0.15	0.08	0.05
B2	3.99	7.42	-1.22	-4.37	-	-	0.08	0.30	0.07	0.05
	5.89	7.19	-1.91	-4.06	0.23	0.10	0.03	0.19	0.08	0.03
Van der Waals		ψ	λ_m	a	g_1	g_2	g_3	g_4	g_5	g_6
		MPa			τ_1=0.003s	τ_2=0.03s	τ_3=0.3s	τ_4=3s	τ_5=30s	τ_6=300s
B1		1.60	2.86	1.49	-	-	0.03	0.38	0.05	0.07
		2.31	2.85	1.51	0.08	0.22	0.07	0.22	0.03	0.05

using the iterative non-linear Generalized Reduced Gradient (GRG) solver provided in Microsoft Excel.

Great care was taken to make the procedure sufficiently robust, and to ensure that the number of data points considered was balanced for the different test types, occurring over widely different timeframes ranging from about 1 s (for the fastest ramp at 0.6 s^{-1}) to 300 s (for relaxation tests). A load-based sampling would not result in a sufficiently accurate description of the relaxation plateau; therefore, the optimal choice was to use a time-based sampling with an interval of 0.1 s for the relaxation tests and the lowest speed ramp (0.006 s^{-1}), 0.01 s and 0.001 s for the ramps at 0.06 s^{-1} and 0.6 s^{-1}, respectively.

Initially a number of 4 terms was selected for the Prony series in Equation 4, with coefficients τ_i representing the characteristic times of the relaxation spectrum arbitrarily chosen as 0.3 s, 3 s, 30 s and 300 s. These values are uniformly (in log-scale) spread over the time range of interest, as reported by several works in the literature (e.g. Lai & Bakker 1995).

All the remaining parameters (the weights g_i in the Prony series and the coefficients of the hyperelastic models) were thus identified for each material, considering different hyperelastic potentials (Mooney-Rivlin, Ogden with N=1 or 2, Van der Waals). For each material, the optimal set is reported in Table 1.

5 NUMERICAL MODELLING

The compression test of the complete track specimen has been simulated using the commercial FE code Abaqus in which displacements were imposed according to the specified loading history. The two rubbery materials were modelled using:

- *Top layer:* eight-node hexahedral elements with reduced integration, hourglass control and hybrid formulation (C3D8RH)
- *Bottom layer:* four-node tetrahedral elements with hybrid formulation (C3D4H)

Perfect bonding was assumed between the two parts, as shown in Figure 1. A mesh sensitivity

analysis was performed to identify the optimal element size for the base layer, set at 2 mm side to account for the more complex honeycomb geometry.

Each constituent material (F2 and B1) was described according to the constitutive model presented in section 4. However, to acknowledge the effect of material porosity (absent in the samples used for the model calibration), the parameters listed in Table 1 (considering the 4-terms Prony series) have been rescaled: the track sample was treated as a composite material made by a continuous elastomeric matrix (corresponding to the constituent properties, as identified so far) and a dispersed void phase, whose volume fraction ϕ_d was estimated according to the density measurements reported above. The generalized form of Kerner equation for inverted systems (Kerner 1956) was used to this purpose:

$$\frac{G_c}{G} = \frac{1-(1+0.47\phi_d)\phi_d}{1+\frac{2}{3}\phi_d} \qquad (10)$$

where G and G_c are the matrix and composite shear moduli, respectively. Equation 9 was derived by assuming values of 0.74 for the maximum packaging factor, 0.50 for the Poisson's ratio of the matrix, and 0 for the modulus of the dispersed phase. The obtained scaling factor G_c/G was applied to the coefficients of the hyperelastic potential for the two constituent materials, as reported in Table 2. Results of the simulations are shown in Figure 3.

Table 2. Corrected hyperelastic parameters.

Material	ϕ_d	G_c/G	μ_1	α_1	ψ	λ_m	a
	%		MPa		MPa		
F2	28.3	0.57	1.90	2.62			
B1	26.3	0.60			0.96	2.86	1.49

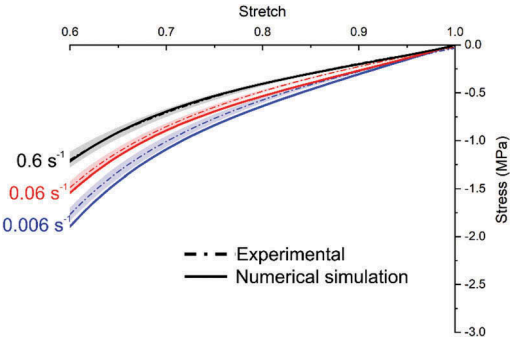

Figure 3. Comparison of experimental data and numerical simulations of the compression tests of the complete track.

6 UPDATED IDENTIFICATION PROCEDURE

The inclusion of a viscoelastic component should make the constitutive model able to predict the material behavior at any given strain rate. However, the model is phenomenological and a limitation intrinsic to the current identification procedure is the time window of the available experimental data.

Dynamic conditions, such as those experienced by a typical track during testing with the AA, involve stretch rates up to 60 s^{-1} (Andena et al. 2015), in which the material response is governed by characteristic times which are far smaller than the range currently considered in the experiments used for model calibration. To overcome this limitation, an approach similar to the one previously proposed in Andena et al. 2018a has been adopted. A virtual curve at 60 s^{-1} was generated by fitting and extrapolating the available data from compression curves at each stretch value in the range between 0.6 and 1, spaced by 0.01 intervals. An example of this linear (in semi-logarithmic scale) extrapolation procedure and of the virtual generated curve is shown in Figure 4.

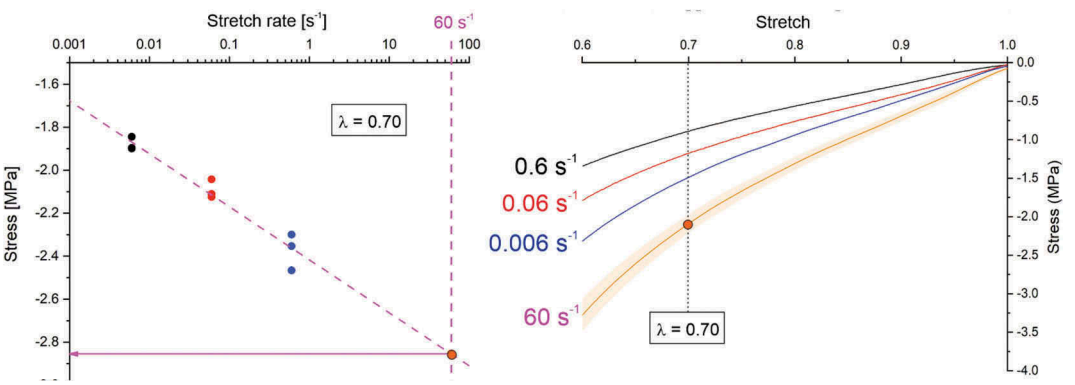

Figure 4. Example of virtual curve generation for material F1 and λ = 0.70 (left); comparison of the complete virtual curve with the relevant averaged experimental ones from which it was generated. The shaded area represents the 95% confidence interval of the extrapolation procedure.

Its application allowed the introduction of two additional terms in Equation 4, whose characteristic times were set at 0.003 and 0.03 s; the relevant coefficients, together with updated values of all the other model parameters, were determined by performing a new calibration on the combined experimental and virtual dataset and are reported in Table 1. To reduce the possible influence of virtual data in the time range for which experimental data are available, a limited number of data points (40, as opposed to about 700 for the other rates) was considered for curve at 60 s^{-1}: in this way, the virtual data basically affected the behavior only at very short times.

7 VALIDATION UNDER DYNAMIC LOADING

The final validation of the proposed model was performed by simulating shock absorption tests, performed using an AA according to EN 14808 standard, prescribed by World Athletics (WA) for track approval and described in detail elsewhere (Andena et al. 2015, 2018a, Benanti et al. 2013). Schematics of the testing setup as represented in

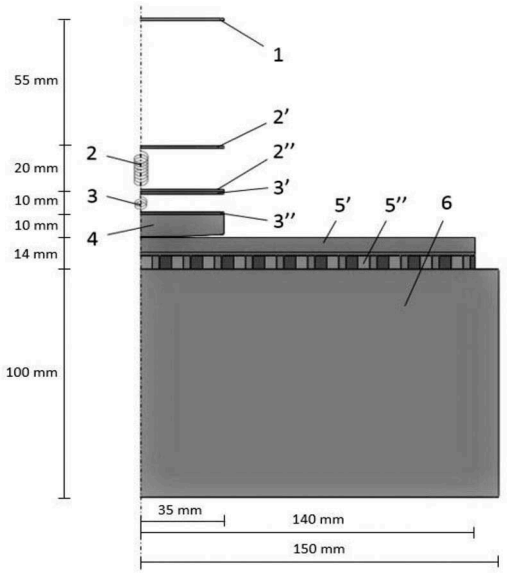

Figure 5. 3D numerical model representing the AA test: 1) Dropping mass; 2) spring (2′ upper and 2" lower plates); 3) load cell (3′ upper and 3" lower plates); 4) test foot; 5) track (composed by 5′ finishing and 5" base layers; 6) substrate.

the 3D FE model are given in Figure 5. The AA records the force measured by a load cell upon the fall of a dropping mass over the spring and testing foot assembly, resting on the track material which is in turn laid on a rigid substrate (e.g. concrete). The purpose of this device is to mimic the first strike of the foot on the ground while running.

To investigate the improvements provided by the present visco-hyperelastic constitutive model, FE numerical simulations were compared with those obtained by using a purely (i.e. with no viscoelastic component) hyperelastic one, whose parameters are reported in Table 3; they were determined by fitting the virtual curve at 60 s^{-1}, following the same approach proposed in Andena et al. 2018a.

Table 3. Parameters of the purely hyperelastic model.

Material	μ_1	α_1	μ_2	α_2	ψ	λ_m	a
	MPa		MPa		MPa		
F1	2.18	2.29					
F2	3.83	2.33					
B2	6.12	8.75	-2.13	-4.90			
B1					2.31	2.66	1.78

Both sets of results were evaluated with reference to the actual data gathered from shock absorption experiments. Results for the four separate materials (F1, F2, B1 and B2) are shown in Figure 6; for better clarity, experimental and numerical data were filtered using a low-pass, ninth order Butterworth filter as defined by WA regulations. In general, both numerical models ensure a good agreement with the experiments. For F1 and B1 a minor overestimation of the force during loading phase, as well as a lower peak force, can be observed. The post-peak response is where the two numerical models differ: while both slightly overestimate the force during the unloading phase, the visco-hyperelastic one clearly provides an improvement over the previous, purely hyperelastic model. This is not surprising, since the latter lacks a dissipative component which in the real material is already active during the loading phase, thus implicitly incorporating its effect in the hyperelastic parameters, which are identified on the basis of the compression data (with no unloading). The newly developed visco-hyperelastic model, in turn, features an inherent dissipative component which is responsible for the improved accuracy of the numerical predictions. To quantify this difference, the root mean square error (RMSE) against experimental data was computed on both sets of predicted force vs. time curves.

Its values are reported in Figure 7, with contributions of the loading and unloading phases displayed separately. It is clear that the visco-hyperelastic model provides a marked reduction of the error during unloading, although a gap with the experimental results is still present. Possible causes include the limited validity of the proposed approach (based on the assumption of decoupled hyperelastic and viscoelastic contributions) and an additional dissipative component originated by friction, which should not be neglected even if using PTFE film for lubrication.

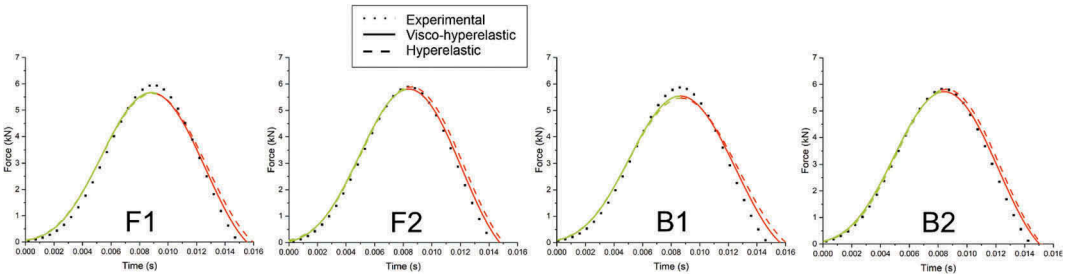

Figure 6. Force vs. time curves from experimental shock absorption tests using the AA and relevant visco-hyperelastic and purely hyperelastic FE models. For each material the loading/unloading parts are indicated in green/red, respectively.

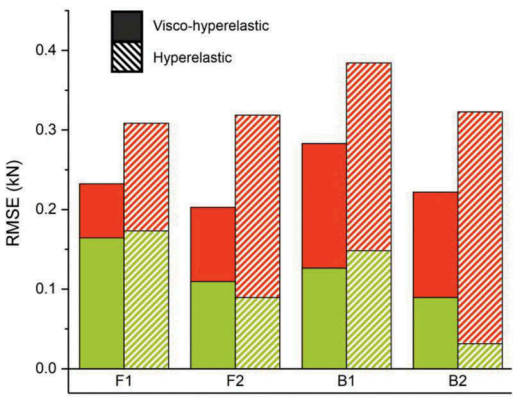

Figure 7. Root mean square error against experimental data of the two numerical models: green (lower) contribution – loading phase; red (upper) contribution – unloading phase.

8 CONCLUSIONS

A combined experimental and numerical approach to identify the constitutive parameters of a time-dependent model for rubbers has been developed. The model is based on decoupled strain and time dependent functions, in turn associated to a hyperelastic potential and Prony series, respectively. Its implementation into standard finite element codes is quite straightforward.

This approach has been tested on four different materials used for athletics tracks, whose constitutive parameters were identified from a set of compression and relaxation experiments performed at varying testing rates. A first validation was obtained by using the model to reproduce compression tests performed (also at varying speeds) on actual track samples, in which the same materials were used to produce a 2-layer structure with a honeycomb geometry. The comparison was successful, provided the originally identified constitutive parameters were corrected to account for the inherent porosity of the track samples.

Finally, the available experimental dataset used for the identification constitutive parameters was updated with the inclusion of a virtual material compression curve, extrapolated at the high strain rates typical of impact conditions. A new set of parameters was identified, accounting for the material behaviour at short times (in the order of milliseconds). They were used to simulate a dynamic test on the complete track, performed experimentally using an artificial athlete.

Results suggest that the present approach produces a visible improvement compared to the previous, purely hyperelastic one. The proposed FE model can thus be exploited to optimize not only shock absorption, but also the energy return characteristics of athletics tracks, sports surfaces and rubber components in general. Its main advantage lies in the relatively easy implementation within a commercial FE code, possible by combining the available hyperelastic and viscoelastic constitutive models. The experimental effort required for the identification of visco-hyperelastic material parameters is also limited.

The accuracy of the present model will be further improved by analyzing more carefully the contribution of friction.

REFERENCES

Andena, L., Aleo, S., Caimmi, F., Mariani, S., Briatico-Vangosa, F. & Pavan, A. 2016. A 3D Numerical Model for the Optimization of Running Tracks Performance. *Procedia Engineering* 147:854–859.

Andena, L., Briatico-Vangosa, F., Cazzoni, E., Ciancio, A., Mariani, S. & Pavan, A. 2015. Modeling of shock absorption in athletics track surfaces. *Sports Engineering* 18(1):1–10.

Andena, L., Aleo, S., Caimmi, F., Briatico-Vangosa, F., Mariani, S., Tagliabue, S. & Pavan, A. 2018a. Modelling the cushioning properties of athletic tracks. *Sports Engineering* 21(4): 453–463.

Andena, L., Briatico-Vangosa, F., Ciancio, A. & Pavan, A. 2014, A Finite Element Model for the Prediction of Force Reduction of Athletics Tracks, *Procedia Engineering* 72(0): 847–852.

Andena, L., Ciancio, A., Briatico-Vangosa, F., Mariani, S. & Pavan, A. 2018b. On the relationship between force reduction, loading rate and energy absorption in athletics tracks. *Proceedings of the Institution of Mechanical Engineers, Part P: Journal of Sports Engineering and Technology* 232(2):71–78.

Baroud, G., Nigg, B.M. & Stefanyshyn, D. 1999. Energy storage and return in sport surfaces. *Sports Engineering* 2:173–180.

Bazkiaei, A.K., Shirazi, K.H. & Shishesaz, M. 2020. A framework for model base hyper-elastic material simulation. *Journal of Rubber Research* 23(4): 287–299.

Benanti, M., Andena, L., Vangosa, F.B. & Pavan, A. 2013. Viscoelastic behavior of athletics tracks surfaces in relation to their force reduction. *Polymer Testing* 32:52–59.

Busfield, J.J.C., Deeprasertkul, C. & Thomas, A.G. 2000. The effect of liquids on the dynamic properties of carbon black filled natural rubber as a function of pre-strain. *Polymer* 41(26): 9219–9225.

Carleo, F., Barbieri, E., Whear, R. & Busfield, J.J.C. 2018. Limitations of Viscoelastic Constitutive Models for Carbon-Black Reinforced Rubber in Medium Dynamic Strains and Medium Strain Rates. *Polymers* 10(988):1–25.

Carré, M.J., James, D.M. & Haake, S.J. 2006, Hybrid Method for Assessing the Performance of Sports Surfaces During Ball Impacts. *Proceedings of the Institution of Mechanical Engineers, Part L: Journal of Materials Design and Applications* 220(1): 31–39.

Cole, D., Forrester, S. & Fleming, P. 2018, Mechanical Characterisation and Modelling of Elastomeric Shockpads. *Applied Sciences* 8(501): 1–13.

De Tommasi, D., Puglisi, G., Toma, E. & Trentadue, F. 2019. A predictive model for the hysteretic and damage behavior of rubberlike materials. *Journal of Rheology* 63(1):1–10.

Goh, S.M., Charalambides, M.N. & Williams, J.G. 2004. Determination of the Constitutive Constants of Non-Linear Viscoelastic Materials. *Mechanics of Time-Dependent Materials* 8(3):255–268.

Kerner E.H. 1956. The Elastic and Thermoelastic Properties of Composite Media. *Proceedings of the Physical Society Section B* 69:808–813.

Kobayashi, K. & Yukawa, H. 2011. Identification of the Exponential Function Type Nonlinear Voigt Model for Sports Surfaces by Using a Multi-Intensity Impact Test. *Journal of System Design and Dynamics* 5(6): 1326–1336.

Lai, J. & Bakker, A. 1995. Analysis of the non-linear creep of high-density polyethylene. *Polymer* 36(1): 93–99.

McMahon, T.A. & Greene, P.R. 1979, The influence of track compliance on running. *Journal of Biomechanics* 12(12): 893–904.

Nigg, B.M. & Yeadon, M.R. 1987. Biomechanical aspects of playing surfaces. *Journal of sports sciences* 5 (2):117–145.

Thomson, R.D., Birkbeck, A.E. & Lucas, T.D. 2001. Hyperelastic modelling of nonlinear running surfaces. *Sports Engineering* 4:215–224.